The Structural Phase Transition in $CaAl_4$: A Concerted Application of Landau Theory and Energy Band Theory

Gordon J. Miller,* Fan Li, and Hugo F. Franzen

Contribution from the Department of Chemistry and Ames Laboratory-DOE, Iowa State University, Ames, Iowa 50011

Received November 18, 1992

Abstract: $CaAl_4$ undergoes a reversible, structural transformation at 170 °C according to high-temperature X-ray powder diffraction experiments. The high-temperature phase adopts the tetragonal $BaAl_4$ structure (space group $I4/mmm$), while the low-temperature phase is monoclinic, $C2/m$, with lattice parameters, a = 6.1526 (15) Å, b = 6.1730 (13) Å, c = 6.3290 (14) Å, β = 118.026 (16)°. The Landau theory of phase transitions correctly provided a structural model for the low-temperature phase, which could be subsequently refined. Also, electronic structure calculations on both forms of $CaAl_4$ allow rationalization of the transformation in terms of changes in local chemical bonding within the Al framework.

Introduction

A fundamental classification of a chemical substance is whether it is metallic or nonmetallic (this is certainly one of the first schemes students learn in introductory classes). Probing the structures and properties of compounds in the "boundary region" between metals and nonmetals has recently become an exciting area in solid-state research. One class of these materials is the polar intermetallics: compounds formed between two or more metallic elements with very different electronegativities whose structures and properties often show aspects of both normal valence compounds as well as typical intermetallics.[1] When the electronegative component is a group 13 element (Al, Ga, or In, in particular), the region between metallic and nonmetallic behavior is not a well-defined line.[2] The consideration of such compounds has led to an increased understanding of chemical bonding and the relationship between geometrical and electronic structure in solids.[3]

In a recent theroetical investigation of alkali metal gallides, Burdett and Canadell suggested that a value of 3.5 valence electrons per electronegative atom represents the critical electron count which separates the formation of deltahedral clusters (common to boranes and carboranes) from open network structures (typical valence compounds).[4] The compounds AX_4, in which A is an alkaline-earth metal and X is a group 13 element, fall exactly at this critical electron count.[5] They adopt a tetragonal unit cell, and their structures show aspects of multicenter electron-deficient bonding as well as two-center, two-electron interactions. In 1979, Zogg and Schwellinger reported that $CaAl_4$ undergoes a martensitic transformation at 140 °C to give a low-temperature modification with monoclinic symmetry.[6] However, no structural details were provided.

Pearson writes that "martensitic transformations...occur because of mechanical instability in the crystal lattice resulting from some internal stress, or from electronic instability resulting from the appearance of a distorted structure of lower free energy".[7] Therefore, in $CaAl_4$ does the observed symmetry reduction have electronic or mechanical origin, or even both? Molecular chemists are well aware of structural instabilities that can be traced back to symmetry characteristics of ground and low-lying excited states via the Jahn–Teller theorems.[8] In this article, we describe the synthesis and structural characterization of $CaAl_4$, both in its low- and high-temperature forms. In particular, the Landau theory of second-order phase transitions provides a structural model for refinement of both powder and single-crystal X-ray diffraction data. In addition, we have closely examined the electronic structure of $CaAl_4$ to elucidate any electronic driving forces for this transformation.

Experimental Section

Sample Preparation. Starting elements consisted of aluminum shot and a calcium ingot at the molar ratio of 4:1 Al/Ca. Since $CaAl_4$ melts peritectically at 700 °C, the synthesis was carried out in two steps in order to acquire a pure specimen. In the first step, the Al–Ca mixture was sealed in a high-purity tantalum ampoule under Ar atmosphere, and then placed into a furnace preheated to 1000 °C. After melting for 25 min (before the tantalum becomes oxidized), the ampoule was quenched in liquid nitrogen. The X-ray diffraction (XRD) pattern shows the initial product to be a mixture of $CaAl_4$, $CaAl_2$, and Al, of which $CaAl_4$ is the major component. This first step can also be performed by arc-melting the Al–Ca mixture under an Ar atmosphere. In the second step, the initial product mixture was sealed in an evacuated quartz ampoule, annealed at a few degrees below the peritectic melting temperature (685 °C) for 30 days, and finally cooled down slowly to room temperature. The final XRD pattern indicated that only traces of $CaAl_2$ and Al remained in the product.

In Situ High-Temperature Powder X-ray Diffraction (HTXRD). The powder XRD data of the $CaAl_4$ sample between room temperature and 600 °C were collected in situ using a high-temperature powder diffractometer with a rotating anode, Cu Kα source, a multifunctional cylindrical chamber, and a gas-flow proportional position sensitive detector. The sample holder was a Mo strip with a depression of 10 mm × 6 mm × 1.5 mm in the center for the fine powder sample. A chromel–alumel thermocouple was spot welded to the center of the bottom of the depression. The temperatures were controlled using a RE2400 thermocontroller with a precision of 0.01 mV. Temperature fluctuations in the sample region are less than 5 °C.[9] In addition, the experiment was run under a pressure of 10^{-7} Torr. Using this diffractometer a satisfactory pattern can be obtained in about 30 s, but the collection time for all patterns shown was set to 3 min in order to improve the counting statistics.

(1) Schäfer, H. *Annu. Rev. Mater. Sci.* **1985**, *15*, 1.
(2) Schäfer, H.; Eisenmann, B.; Müller, W. *Angew. Chem., Int. Ed. Engl.* **1973**, *12*, 694.
(3) Nesper, R. *Angew. Chem., Int. Ed. Engl.* **1991**, *30*, 789.
(4) Burdett, J. K.; Canadell, E. *J. Am. Chem. Soc.* **1990**, *112*, 7207.
(5) Villars, P.; Calvert, L. D. *Pearson's Handbook of Crystallographic Data for Intermetallic Phases*; American Chemical Society for Metals: Metals Park, Ohio, 1985.
(6) Zogg, H.; Schwellinger, P. *J. Mater. Science (London)* **1979**, *14*, 1923.
(7) Pearson, W. B. *The Crystal Chemistry and Physics of Metals and Alloys*; Wiley-Interscience: New York, 1972.
(8) Burdett, J. K. *Moleculer Spaes*; Wiley-Interscience: New York, 1980.
(9) Polonka, J.; Xu, M.; Li, Q.; Goldman, A. I.; Finnemore, D. K. *Appl. Phys. Lett.* **1991**, *59* (27), 3640.

0002-7863/93/1515-3739$04.00/0

Table I. Atomic Parameters for Extended-Hückel Calculations

atom	orbital	H_{ii} (eV)	ζ
Ca	4s	−7.00	1.10
	4p	−4.00	1.10
Al (4d)	3s	−12.30	1.55
	3p	−6.50	1.47
Al (4e)	3s	−12.30	1.37
	3p	−6.50	1.36

Single-Crystal X-ray Diffraction. In order to improve the quality of single crystals, the sample was annealed once again in an evacuated quartz ampoule at the temperature where the phase transformation takes place. The sample was heated at 120 °C for 10 h, and at 200 °C for 30 min, and then the temperature was lowered at a gradual rate of 5 °C/h to 125 °C. It was held at 125 °C for 3 days and, finally, was cooled very slowly to room temperature.

Single-crystal X-ray diffraction was carried out on a Rigaku AFC6 four-circle diffractometer with monochromated Mo Kα radiation. The orientation matrix and lattice parameters for the crystal were determined from 25 reflections in the range $35° < 2\theta < 40°$. Subsequent data reduction and structure refinement were performed with the TEXSAN program package. Of 838 measured reflections, 132 unique reflections ($I \geq 4\sigma(I)$) were used for the structure determination.

Electronic Structure Calculations. The electronic structures of tetragonal and monoclinic $CaAl_4$ were evaluated within the tight-binding approximation (LCAO method) using the extended-Hückel ansatz.[10] Off-diagonal Hamiltonian matrix elements were calculated by the weighted Wolfsberg–Helmholz expression.[11] Energy densities of states (DOS) and crystal orbital overlap population (COOP) curves[12] were determined by summation over a special points set (220 **k**-points in the tetragonal cell; 344 **k**-points in the monoclinic cell) in the irreducible wedge of the first Brillouin zone.[13]

Atomic orbital parameters are listed in Table I.[14] Two sets of orbital exponents were used for the two symmetry inequivalent Al atoms in the tetragonal structure (space group $I4/mmm$). The exponents for Al atoms occupying the 4d (1/2, 0, 1/4) sites were chosen by fitting the experimental band structure (in particular, the splitting at the X point) of Al.[15] We justify the assignment because, when the same parameters are used for both Al sites, we find Mulliken charges of −0.09 for the 4d position and −0.73 for the 4e positions (0, 0, $z \sim 0.38$). Furthermore, identical parameter sets for these two Al sites lead to an energy gap between occupied and unoccupied bands. With the parameters in Table I, $CaAl_4$ should be metallic, and the Mulliken charges become −0.25 at the 4d sites and −0.53 at the 4e sites.

Results

HTXRD. The powder diffraction (Figure 1) and single-crystal X-ray (Tables II, III, and IV) results are consistent with a phase transition, with the room-temperature phase having a broken symmetry relative to the high-temperature phase with $I4/mmm$ symmetry.

Before the high-temperature run, the room-temperature diffraction pattern of the sample was consistent with $C2/m$ symmetry as indicated by peak splitting relative to the pattern corresponding to $I4/mmm$ symmetry. As the temperature was stepped up to 200 °C, the split lines steadily converged, and at 250 °C, all lines can be indexed on the basis of the tetragonal structure of $CaAl_4$. Thus, a transition, possibly continuous, from $C2/m$ to $I4/mmm$ occurs as the sample temperature is increased in this interval. At 200 °C, the temperature was further ramped up to 600 °C at about 10 °C/min, and at every 50 °C interval, a scan was performed. These patterns showed essentially no change except for changes in the relative peak intensities and expected shifts arising from thermal expansion. When the temperature was

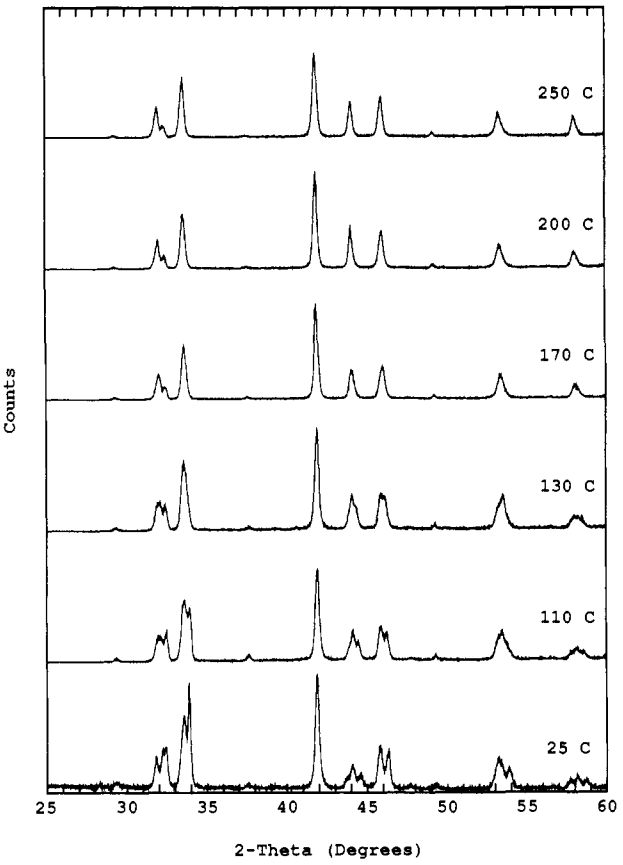

Figure 1. A series of powder diffraction patterns of $CaAl_4$ taken at the indicated temperatures between room temperature and 270 °C.

Table II. Crystal Data

formula	$CaAl_4$
formula weight	148.01
space group	$C2/m$
a, Å	6.1526(15)
b, Å	6.1730(13)
c, Å	6.3290(14)
α, deg	90
β, deg	118.026(16)
γ, deg	90
V, Å^3	212.190(89)
Z	2
d_{calc}, g/cm^3	2.316
crystal size, mm	0.05 × 0.06 × 0.07
μ(Mo Kα), cm^{-1}	20.435
data collection instrument	Rigaku AFC6
radiation (monochromated in incident beam)	Mo Kα (λ = 0.710 69 Å)
orientation reflections, number, range (2θ)	25, $35.32 < 2\theta < 39.76°$
temperature, °C	23
scan method	$\omega - 2\theta$
data col range, 2θ, deg	6–50
no. data collection	838
no. unique data, total:	424
with $I > 4.00\sigma(I)$:	132
no. of parameters refined	17
trans. factors, max, min (ψ-scans)	0.7135–1.000
R^a	0.059
$R_w{}^b$	0.064
quality-of-fit indicator^c	2.09
largest shift/esd, final cycle	0.00, 1
largest peak, e/Å^3	0.841 (−0.701)

$^a R = \sum||F_o| - |F_c||/\sum|F_o|$. $^b R_w = [\sum w(|F_o| - |F_c|)^2/\sum w|F_o|^2]^{1/2}$; $w = 1/\sigma^2(|F_o|)$. ^{c} Quality-of-fit = $\sum((|F_o| - |F_c|)/\sigma)/(N_{obs} - N_{parameters})$.

(10) (a) Hoffmann, R. *J. Chem. Phys.* **1963**, *39*, 1397. (b) Hoffmann, R.; Lipscomb, W. N. *J. Chem. Phys.* **1962**, *36*, 2179. (c) Hoffmann, R.; Lipscomb, W. N. *J. Chem. Phys.* **1962**, *37*, 2872. (d) Whangbo, M.-H.; Hoffmann, R.; Woodward, R. B. *Proc. R. Soc. London* **1979**, *A366*, 23.

(11) Ammeter, J. H.; Bürgi, H.-B.; Thibeault, J. C.; Hoffmann, R. *J. Am. Chem. Soc.* **1978**, *100*, 3686.

(12) Wijeyesekera, S. D.; Hoffmann, R. *Organometallics* **1984**, *3*, 949.

(13) Chadi, D. J.; Cohen, M. L. *Phys. Rev. B.* **1973**, *8*, 5747.

(14) Alvarez, S. *Tables of Parameters for Extended-Hückel Calculations*, private communication.

(15) Levinson, H. J.; Greuter, F.; Plummer, E. W. *Phys. Rev. B.* **1983**, *27*, 727.

Table III. Positional Parameters and Equivalent Isotropic Thermal Parameters, B(eq), for Monoclinic $CaAl_4$

atom	x	y	z	B(eq)
Ca(1)	0	0	0	1.4(2)
Al(1)	0	0.7592(9)	1/2	1.5(2)
Al(2)	0.3953(8)	0	0.7720(9)	1.3(2)

Table IV. Anisotropic Thermal Parameters, U_{ij}, for Monoclinic $CaAl_4$

atom	U_{11}	U_{22}	U_{33}	U_{12}	U_{13}	U_{23}
Ca(1)	0.012(2)	0.014(3)	0.024(3)	0	0.006(2)	0
Al(1)	0.016(2)	0.018(3)	0.020(2)	0	0.007(2)	0
Al(2)	0.014(2)	0.011(3)	0.020(3)	0	0.005(2)	0

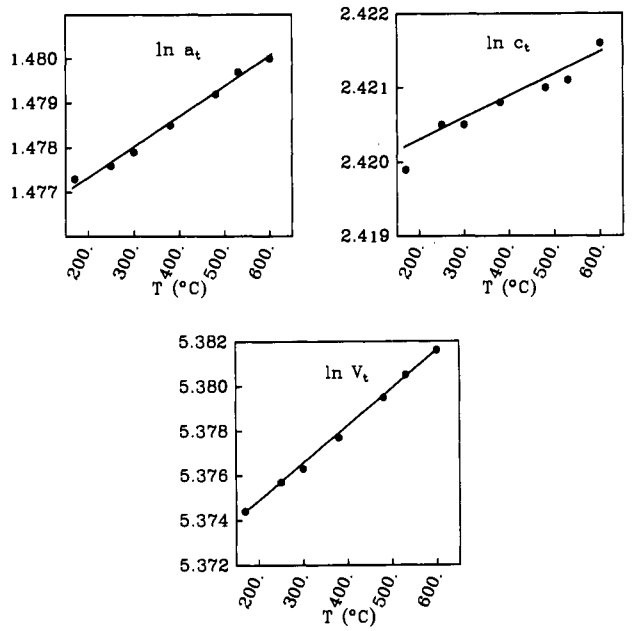

Figure 2. Variation of ln a_t, ln c_t, and ln V_t with temperature for the tetragonal $CaAl_4$ phase between 200 °C and 600 °C.

ramped down from 600 °C, scans were performed at the same temperature stages as in the upward direction. At about 170 °C, peak splitting began to appear, and the original room-temperature pattern was recovered at 25 °C, indicating that the sample regained its original structure.

Although the nature of the peak splittings in the monoclinic system makes exact assignment of 2θ values tenuous, we were able to evaluate lattice parameters for the high-temperature tetragonal phase between 200 °C and 600 °C. Figure 2 illustrates the variation of ln a_t, ln c_t, and ln V_t with temperature. Both ln a_t and ln V_t exhibit linear relations, while ln c_t becomes nonlinear near the transition point. From the slope of ln V_t versus T, we obtain an approximate value for the linear coefficient of thermal expansion, $\alpha_0^L = 0.056 \times 10^{-4}\ K^{-1}$, over the range 200 to 600 °C. This value is four times smaller than α_0^L for Al metal,[16] and indicates the influence of local chemical bonding effects in $CaAl_4$.

A possible concern is whether the entire sample is at thermal equilibrium when each scan is performed. Actually, at every temperature stage, the sample was held at constant temperature for 10 min before the scan was taken, and the sample was held for 1 h at 170 °C and 400 °C, respectively. No significant changes in the patterns were detected. Another question is whether the phase transformation can occur when the temperature vaults over a large span. This effect was positively confirmed when the temperature was raised from 25 to 135 °C, and then from 135° to 200 °C within less than 20 s, or lowered from 200 °C to room temperature.

(16) Callen, H. B. *Thermodynamics*; John Wiley: New York, 1960; p 350.
(17) Landau, L. D.; Lifshitz, E. M. *Statistical Physics*; Pergamon Press: London, 1958.

Table V. The Centrosymmetric Small Representation of $I4/mmm$ at the Γ Point

ε	C_{2z}	C_{2y}	C_{2x}	$C_{2(x+y)}$	$C_{2(y-x)}$	C_{4z}	C_{4z}^2
$\begin{pmatrix}1&0\\0&1\end{pmatrix}$	$\begin{pmatrix}-1&0\\0&-1\end{pmatrix}$	$\begin{pmatrix}1&0\\0&-1\end{pmatrix}$	$\begin{pmatrix}-1&0\\0&1\end{pmatrix}$	$\begin{pmatrix}0&1\\1&0\end{pmatrix}$	$\begin{pmatrix}0&-1\\-1&0\end{pmatrix}$	$\begin{pmatrix}0&-1\\1&0\end{pmatrix}$	$\begin{pmatrix}0&1\\-1&0\end{pmatrix}$
i	σ_z	σ_y	σ_x	σ_{x-y}	C_{y-x}	$\bar{C}_{4z}$	$\bar{C}_{4z}^2$
$\begin{pmatrix}1&0\\0&1\end{pmatrix}$	$\begin{pmatrix}-1&0\\0&-1\end{pmatrix}$	$\begin{pmatrix}1&0\\0&-1\end{pmatrix}$	$\begin{pmatrix}-1&0\\0&1\end{pmatrix}$	$\begin{pmatrix}0&1\\1&0\end{pmatrix}$	$\begin{pmatrix}0&-1\\-1&0\end{pmatrix}$	$\begin{pmatrix}0&-1\\1&0\end{pmatrix}$	$\begin{pmatrix}0&1\\-1&0\end{pmatrix}$

Landau Theory. The first consideration in Landau theory is the determination of whether or not a wave vector ($\bar{\mathbf{k}}$) (or set of equivalent wave vectors in a star) corresponds to the distortion in the sense that any lost translations (vectors $\bar{\mathbf{T}}_i$) yield nonintegral values for ($\bar{\mathbf{k}}\cdot\bar{\mathbf{T}}_i/2\pi$). Since there is no superstructure created by the distortion to monoclinic in $CaAl_4$, the $\bar{\mathbf{k}}$ vector to which the distortion corresponds is $\bar{\mathbf{k}} = \bar{\mathbf{0}}$. The second consideration is the determination of whether the symmetry change corresponds to a small representation of the group of symmetry operations to which $\bar{\mathbf{k}}$ is invariant modulo a reciprocal lattice vector. Since the wave vector under consideration is $\bar{\mathbf{k}} = \bar{\mathbf{0}}$, the small representations to be considered are the irreducible representations of the point group isomorphous to the crystal class, i.e., the irreducible representations of D_{4h}.

There are a number of one-dimensional representations (all except the totally symmetric) that result in a loss of all symmetry operations with character −1, i.e., which lead according to Landau theory to a halving of the number of rotational symmetry operations, and thus to space groups with eight essential symmetry operations. These transitions may occur as second-order transitions. However, monoclinic space groups have at most four essential symmetry operations, and thus the transition under consideration, if it occurs continuously, must correspond to one of the two two-dimensional irreducible representations. The two-dimensional small representation at the Γ point ($\bar{\mathbf{k}} = \bar{\mathbf{0}}$) that is symmetric with respect to inversion is shown in Table V. As a first attempt, it was anticipated that the resultant, monoclinic structure would be centrosymmetric, and, therefore, the symmetry consequences of this irreducible representation were determined.

The third consideration of Landau theory is to determine whether any third-order combination of basis vectors is invariant under all symmetry operations of the group. If such a third-order invariant exists, then a third-order term appears in the Gibbs free energy expansion in the order parameter η, and the transition must be discontinuous.[18] For the case of a two-dimensional irreducible representation the particle density, ρ, can be expressed in terms of that for the symmetrical form, ρ^0, and the two basis functions, ϕ_1 and ϕ_2:

$$\rho = \rho^0 + (\phi_1 + \phi_2)\eta$$

This function is symmetric with respect to the operations of $C2/m$ with $\bar{\mathbf{a}}_m \cong \bar{\mathbf{a}}_t - \bar{\mathbf{b}}_t$, $\bar{\mathbf{b}}_m \cong \bar{\mathbf{a}}_t + \bar{\mathbf{b}}_t$, and $\bar{\mathbf{c}}_m \cong (\bar{\mathbf{a}}_t - \bar{\mathbf{b}}_t + \bar{\mathbf{c}}_t)/2$. This choice of axes follows from the fact that the unique

(18) See, for example, the discussion in: Franzen, H. F. *Chem. Mater.* **1990**, *2*, 486.

Table VI. Lifshitz Analysis of the Centrosymmetric Two-Dimensional Small Representation of $I4/mmm$ at Γ

g	ϵ	C_{2z}	C_{2y}	C_{2x}	$C_{2(x+y)}$	$C_{2(y-x)}$	C_{4z}	C_{4z}^2
$\chi(g)$	2	−2	0	0	0	0	0	0
$\chi^2(g)$	4	4	0	0	0	0	0	0
$\chi(g^2)$	2	2	2	2	2	2	−2	−2
$\chi^2(g) - \chi(g^2)$	2	2	−2	−2	−2	−2	2	2
$V(R)$	3	−1	−1	−1	−1	−1	1	1
g	i	σ_z	σ_y	σ_x	σ_{x+y}	σ_{y-x}	$\bar{C}_{4z}$	$\bar{C}_{4z}^2$
$\chi(g)$	2	−2	0	0	0	0	0	0
$\chi^2(g)$	4	4	0	0	0	0	0	0
$\chi(g^2)$	2	2	2	2	2	2	−2	−2
$\chi^2(g) - \chi(g^2)$	2	2	−2	−2	−2	−2	2	2
$V(R)$	−3	1	1	1	1	1	−1	−1

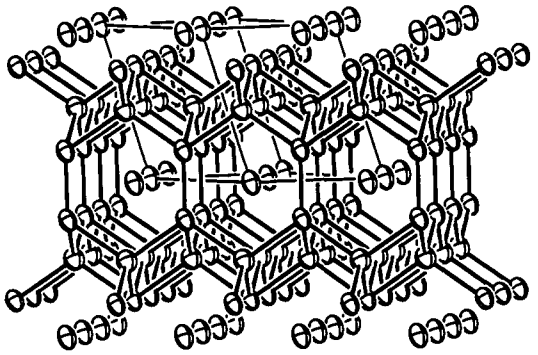

Figure 3. The room-temperature structure ($C2/m$ symmetry) of $CaAl_4$. Short interatomic contacts within the Al network are indicated; 95% thermal ellipoids are drawn.

2-fold axis that takes $\phi_1 + \phi_2$ into itself is $C_{2(x+y)}$, as can be seen from Table V. Furthermore, ϕ_1 and ϕ_2 transform into $-\phi_1$ and $-\phi_2$ under C_{2z} (Table V), and thus no third-order invariant combination can be formed from basis functions for this irreducible representation. It follows that $I4/mmm \rightarrow C2/m$ with the lattice given above meets the Landau conditions for a second-order phase transition.[17,18] This space group and lattice predicted by Landau theory have been confirmed by single-crystal X-ray diffraction, as discussed below.

Finally, in order to determine whether a second-order transition is allowed, it must be determined whether the Lifshitz criterion is met. This criterion is used to determine whether a minimum in the Gibbs free energy as a function of wave vectors is fixed by symmetry at the reciprocal space point to which the transition corresponds. In the case under consideration, this condition takes the form[19]

$$\sum_R [\chi^2(g) - \chi(g^2)] \cdot V(R) = 0$$

where the sum is over the operations of the point group of the wave vector (D_{4h} in this case), $\chi(g)$ is the character of the representation of the space group operation g, and $V(R)$ is the character of the vector representation (basis functions: x, y, and z) under the point group operation of D_{4h} corresponding to g. This analysis is carried out in Table VI and shows that the transition meets the Lifshitz condition.

Single-Crystal X-Ray Diffraction. The indexing program used in the single-crystal X-ray data collection straightforwardly yielded the monoclinic lattice and space group predicted by Landau theory for the Γ point distortion. Important details of the data collection and results are presented in Table II, positional parameters and equivalent isotropic thermal parameters are listed in Table III, and the anisotropic thermal parameters are given in the Table IV. Figure 3 shows the room-temperature structure found in this work.

(19) Toledano, J.-C.; Toledano, P. *The Landau Theory of Phase Transition*; World Scientific: Singapore, 1987.

When the inverse transformation of that stated above is applied to the monoclinic cell of $CaAl_4$ the pseudotetragonal cell has a slight distortion of 3.6 ° in the angle γ: a_t and b_t = 4.3578 Å, c_t = 11.176 Å, $\alpha = \beta = 90°$, γ = 93.60°. The values of a_t and c_t are quite close to those reported by Nowotny: a_t = 4.362 Å, c_t = 11.090 Å (5). The corresponding atomic positions in the pseudotetragonal cell are listed in Table VII and show shifts in the Al position along {110} directions with Δ = 0.009. The resulting displacement vectors correspond to an e_g mode at the Γ point, and Al(1) transforms into the 4d position, while Al(2) transforms into the 4e positions (z = 0.386) of the tetragonal structure. In further discussions, Al(1m) and Al(2m) refer to atoms in the monoclinic structure, while Al(1t) and Al(2t) correspond to the 4d and 4e sites, respectively, in the tetragonal phase.

Discussion

The structural transition observed and clarified for $CaAl_4$ represents another example of symmetry-breaking transformations in intermetallic compounds, as in the cases of VIr[20] and RhTi.[21] And, as in these two examples, the Landau theory provides a structural model for the lower symmetry phase from which we obtain refinement of the single-crystal data of $CaAl_4$. In our view, the most important consequence of the results reported above is that they raise the question: are there underlying electronic forces driving this transition?

In two recent articles, Zheng and Hoffmann[22] as well as Burdett and Miller[23] examined the orbital interactions in $BaAl_4$ and indicated that 14 electrons per formula unit is the optimal valence electron concentration for the tetragonal structure. To summarize their analysis of the chemical bonding: two-center, two-electron bonds occur between adjacent Al(2t) atoms, while multicenter electron-deficient bonding takes place in each tetragonal pyramid formed by four Al(1t) sites and one Al(2t) site. In terms of a fragment orbital analysis, electron-deficient PbO-type $[Al_4]^{2-}$ layers are bonded together via two-electron σ interactions between apical Al(2t) atoms on adjacent layers. We can use localized orbitals to elaborate on their ideas. To count valence electrons, we treat each Ca as a two-electron donor to the $[Al_4]$ framework. Then, since the Mulliken population analysis mentioned earlier indicates a greater negative charge on the Al(2t) atoms, we can formally assign four electrons to each Al(2t) and three electrons to each Al(1t). Furthermore, each Al(1t) is nearly tetrahedrally coordinated by four Al(2t) atoms, whereas each Al(2t) centers a square pyramid of one axial Al(2t) atom and four equatorial Al(1t) sites. Therefore, we utilize sp^3 hybrid orbitals at each Al(1t) site and sp hybrids at Al(2t). Figure 4 (top) shows an orbital interaction diagram at Γ when two isolated PbO-type $[Al_4]^{2-}$ nets (a and c) are brought together to form the complete

(20) Chen, B.; Franzen, H. F. *J. Less-Common Met.* **1990**, *195*, 343.
(21) Yi, S. S.; Chen, B.; Franzen, H. F. *J. Less-Common Met.* **1988**, *143*, 243.
(22) Zheng, C.; Hoffmann, R. *Z. Naturforsch.* **1986**, *41B*, 292.
(23) Burdett, J. K.; Miller, G. J. *Chem. Mater.* **1990**, *2*, 12.

Table VII. Atomic Positions in the Pseudotetragonal Cell for $CaAl_4$

atom	(x_m, y_m, z_m)	(x_t, y_t, z_t)	(x_t^0, y_t^0, z_t^0)	Δ
Ca(1)	0, 0, 0	0, 0, 0	0, 0, 0	0, 0, 0
	$^1/_2, ^1/_2, 1$	$^1/_2, ^1/_2, ^1/_2$	$^1/_2, ^1/_2, ^1/_2$	0, 0, 0
Al(1)	0, 0.7592, $^1/_2$	0.5092, 0.0092, $^1/_4$	$^1/_2, 0, ^1/_4$	(0.0092, 0.0092, 0)
	0, 0.2408, $^1/_2$	–0.0092, 0.4908, $^1/_4$	$0, ^1/_2, ^1/_4$	(–0.0092, –0.0092, 0)
	1, 0.2408, $^3/_2$	0.4908, –0.0092, $^3/_4$	$^1/_2, 0, ^3/_4$	(–0.0092, –0.0092, 0)
	$^1/_2$, 0.2592, $^3/_2$	0.0092, 0.5092, $^3/_4$	$0, ^1/_2, ^3/_4$	(0.0092, 0.0092, 0)
Al(2)	0.3953, 0, 0.7720	0.0093, –0.0095, 0.3860	0, 0, 0.3860	(0.0093, –0.0093, 0)
	0.6047, 0, 1.2280	–0.0093, 0.0093, 0.6140	0, 0, 0.6140	(–0.0093, 0.0093, 0)
	0.1047, $^1/_2$, 0.2280	0.4907, 0.5093, 0.1140	$^1/_2, ^1/_2$, 0.1140	(–0.0093, 0.0093, 0)
	0.8953, $^1/_2$, 1.7720	0.5093, 0.4907, 0.8860	$^1/_2, ^1/_2$, 0.8860	(0.0093, –0.0093, 0)

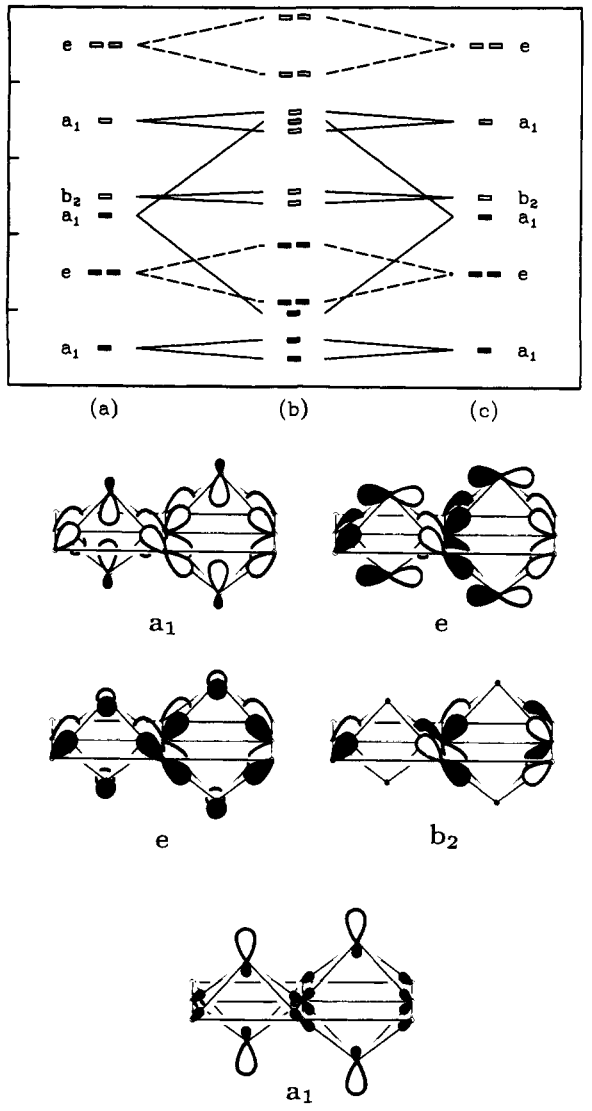

Figure 4. (Top) Localized orbital interaction diagram between two isolated PbO-type $[Al_4]^{2-}$ layers to form the three-dimensional framework in tetragonal $CaAl_4$. Solid lines represent σ or nonbonding overlap and dashed lines indicate π overlap. Occupied orbitals are shaded. (Bottom) Pictorial representation of the five lowest energy localized orbitals within each tetragonal pyramid at the zone center, Γ. The Al(1t) sites have sp^3 hybrids and the Al(2t) sites have sp hybrids. See text for further discussion.

three-dimensional structure (b). In fact, schemes (a) and (c) depict qualitative localized orbital energy diagrams for a single tetragonal pyramid as described above. Since these pyramids share equatorial edges through the Al(1t) sites, and the sp^3 hybrid orbitals assigned to each atom form an orthogonal set, the localized bonding in each tetragonal pyramid may be treated independently of its neighbors.

The five localized bonding and nonbonding orbitals for the two-dimensional fragment are illustrated in Figure 4 (bottom).

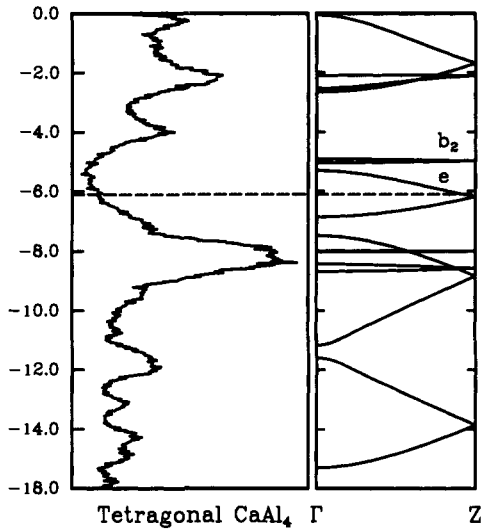

Figure 5. Energy DOS and dispersion curves along the line Γ–Z for tetragonal $CaAl_4$. The Fermi level is indicated by the dashed line.

The low-lying a_1 and e orbitals utilize the inward-pointing sp hybrid and (p_x, p_y) orbitals on Al(2t) to form multicenter bonding orbitals with the basal Al(1t) sp^3 hybrids. The intermediate a_1 level has mostly outward-pointing sp hybrid character on Al(2t), and the b_2 orbital is centered exclusively on the Al(1t) sites (Al(1)–Al(2) nonbonding). The higher a_1 and e levels are the antibonding counterparts of the lower a_1 and e orbitals and are not depicted. In order to count electrons for this orbital scheme, each Al(1t) site is shared among four pyramids and, therefore, contributes $^3/_4$ electron per cluster, while each Al(2t) donates four electrons for a total of seven valence electrons per cluster. When these fragments interact, the most significant orbital overlap occurs between the outward-pointing sp hybrids on adjacent Al(2t) sites to form a bonding and antibonding combination. On the other hand, the intercluster a_1 and e levels interact weakly with neighboring layers, as does the nonbonding b_2 crystal orbital. The result of this qualitative cluster model is that the highest occupied orbitals have e character, and the lowest unoccupied levels have b_2 character. Second-order Jahn–Teller arguments, therefore, predict an e mode ($b_2 \otimes e$) to stabilize the "HOMO" and lead to distortion of the regular pyramid.[8] Qualitatively, this localized picture is consistent with the predictions of Landau theory, but we appeal to a delocalized picture for further details.

Figure 5 illustrates the DOS for tetragonal $CaAl_4$ as well as the dispersion of energy bands from $\Gamma(0,0,0)$ to $Z(0,0,^1/_2)$ in the Brillouin zone. Note that the Fermi level lies just above the 4-fold degeneracy at Z and near a minimum in the DOS; $CaAl_4$ should be metallic. The band crossing the calculated Fermi level has e symmetry in the group of the wave vector **zc***, and the next highest band has b_2 character with only p_z contributions from the Al(1t) atoms and essentially no dispersion along this direction. Second-order Jahn–Teller mixing may occur via a vibrational mode with e symmetry. Since the strength of orbital mixing is inversely proportional to the energy difference between the e and

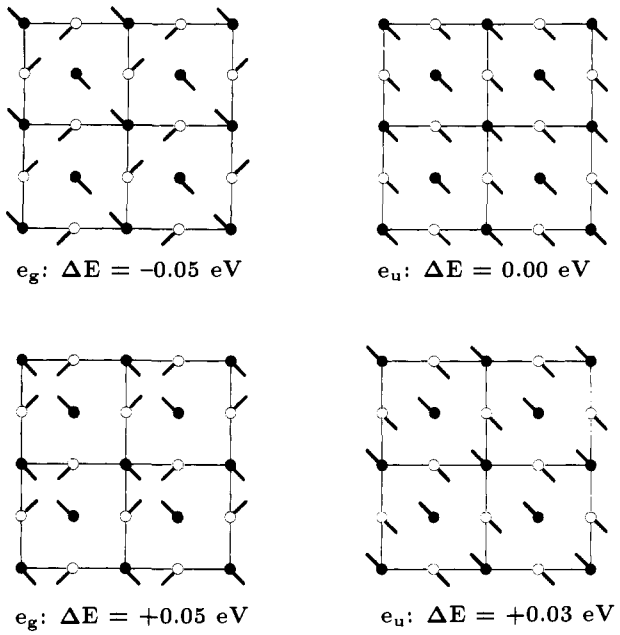

Figure 6. Representations of the doubly degenerate phonon modes at Γ for tetragonal $CaAl_4$. Symmetry labels correspond to the group $4/mmm$ (D_{4h}). ΔE values are with respect to the undistorted structure.

b_2 bands, modes with wave vectors $\mathbf{zc}^*$ for $0 \leq z \leq 1/2$ will have nearly equal magnitudes from a dispersionless "LUMO". Since a direct gap ($\Delta\mathbf{k} = \mathbf{0}$) mode is included in this range, we can classify the Jahn–Teller active modes as either e_g or e_u.

In the primitive tetragonal cell, there are 15 possible modes ($N = 5$ atoms), of which three are translational degrees of freedom at the Γ point. These three modes transform as $a_{2u} + e_u$ under the group $4/mmm$ (D_{4h}). The 12 remaining vibrational modes were determined using group theoretical techniques and all modes are assigned to the three inequivalent sites as follows:

Ca: $a_{2u} + e_u$

Al(1t): $a_{1g} + e_g + a_{2u} + e_u$

Al(2t): $b_{1g} + e_g + a_{2u} + e_u$

Figure 6 illustrates the possible e_g and e_u modes, and also compares the total energy of the distorted structure with the undistorted tetragonal framework. An e_g mode in Figure 6 leads to the only stabilization (by 0.05 eV per formula unit) and is, indeed, the distortion we observe from $I4/mmm \rightarrow C2/m$. When the displacements in the lattice parameters are also considered, the net stabilization of the monoclinic structure becomes nearly 0.2 eV per formula unit. The calculated DOS and dispersion curve in Figure 7 for the monoclinic structure show small changes in the DOS from the tetragonal phase except near the Fermi level, but the degeneracy at the tetragonal Z point is broken. Although group theoretical techniques are sufficiently powerful to identify the symmetry species of the distortion coordinate, a detailed energy band calculation is still required to identify the precise nature of this mode.

Can we understand the nature of the distortion in $CaAl_4$ by changes in local chemical bonding? Nearly 30 years ago, Bruzzone set forth a size argument for the stability of the tetragonal $BaAl_4$ structure type relative to others with similar stoichiometries. From tabulated metallic radii,[24] he showed that, for MX_4 systems, the $BaAl_4$ structure is stable when $R_M:R_X > 1.35$. According to these values, $CaAl_4$ lies close to this border ($R_{Ca}:R_{Al} = 1.41$). In addition, as we mentioned earlier, recent theoretical investigations have also emphasized the importance of valence electron concentration for these structures.[22,23] In the

(24) Bruzzone, G. *Acta Cryst.* **1965**, *18*, 1081.

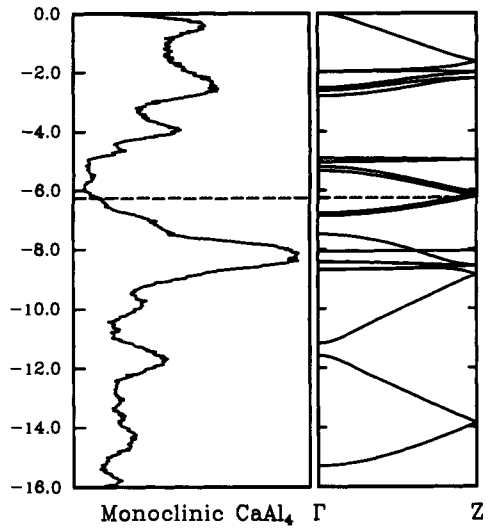

Figure 7. Energy DOS and dispersion curves along the line Γ–Z for monoclinic $CaAl_4$. The Fermi level as indicated by the dashed line.

Table VIII. Structural Parameters in Tetragonal Alkaline-Earth Tetraaluminides

	$CaAl_4$	$SrAl_4$[26]	$BaAl_4$[26]
a (Å)	4.362	4.463	4.566
c (Å)	11.090	11.203	11.278
c/a	2.542	2.510	2.470
V (Å^3)	211.0	223.1	235.1
d(Al–Al) (Å)[a]			
(4d)–(4d)	3.084	3.156	3.229
(4d)–(4e)	2.614	2.665	2.713
(4e)–(4e)	2.662	2.689	2.707
d(M − Al) (Å)[a]			
(2a)–(4d)	3.528	3.581	3.628
(2a)–(4e)	3.359	3.430	3.501
	4.214	4.257	4.286

[a] Atoms labeled according to their Wyckoff symbol.

Ca–Al system, in particular, Hafner argues that the exceptionally high stability of the cubic Laves phase, $CaAl_2$, is due to the fact that the interatomic distances coincide exactly with the minima in the pair potentials.[25] Table VIII indicates that a similar effect is presumably important in the MAl_4 series where M is an alkaline earth metal. Although the unit cell volumes increase by 11% from Ca to Ba, the shorter Al–Al contacts change by 0.045 and 0.099 Å. The most significant changes occur between adjacent Al(1t) sites (0.145 Å) within square nets.

We have analyzed the bonding in tetragonal $CaAl_4$ by choosing the corresponding unit cell volume from the monoclinic room temperature structure, a c/a ratio of 2.50, and varying the z positional parameter of Al(2t). Figure 8 summarizes our results. Evaluation of total electronic energies indicates a minimum energy near $z = 0.376$, in excellent agreement with other reported tetragonal phases.[5] Changing the z parameter leads to converse trends in the Al(2t)–Al(2t) and Al(1t)–Al(2t) distances, and likewise in their overlap populations. However, as z increases, the Al(1t)–Al(1t) distance within the square net remains constant, while its overlap population increases. Thus, the minimum in our total energy curve is mostly due to the optimization of the total Al–Al bonding in the structure.

When we apply the e_g distortion, the most significant distance changes occur in the square nets of Al(1t) atoms: 3.081 ($4x$) → 2.973, 3.078 ($2x$), 3.200 Å. However, the bonding character in the Al(2)–Al(2) apical linkages becomes significantly altered: the overlap population increases from 0.365 in the tetragonal structure to 0.543 in the monoclinic structure, although the change

(25) Hafner, J. *From Hamiltonian to Phase Digrams*; Springer-Verlag: Heidelberg, 1987; p 59.

(26) Bruzzone, G.; Merlo, F. *J. Less-Common Met.* **1975**, *39*, 1.

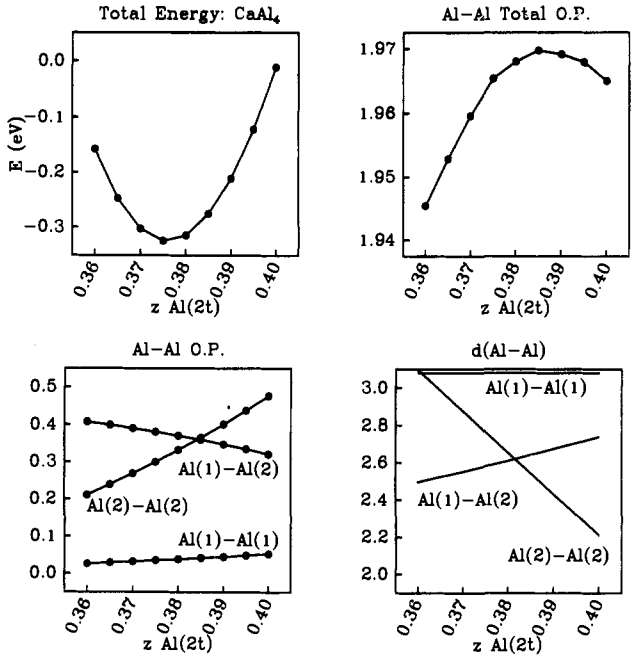

Figure 8. Variations in total electronic energy, individual Al–Al overlap populations, Al–Al distances, and total Al–Al overlap populations for tetragonal $CaAl_4$ as a function of the z-parameter of the Al(2t) sites.

in bond distance is only +0.004 Å. In addition, the Al(1)–Al(2) bonds show a slightly reduced overlap population in the monoclinic phase (0.285 and 0.299 versus 0.359 in the tetragonal phase), and the shortest Al(1m)–Al(1m) distance develops an overlap population of 0.101 (an increase of 0.057 over the tetragonal structure). The strong enhancement of the apical linkages is readily seen from the dispersion curve of the monoclinic system (Figure 7). The 4-fold degeneracy near the Fermi level in the tetragonal structure arises by the folding together of a band which has π-bonding character between apical atoms at the bottom and π-antibonding character at the top.[22,23] The degeneracy occurs at the point where these two effects exactly cancel each other due to the effects of translational symmetry. Upon the e_g distortion, this degeneracy is broken, and π-bonding levels are stabilized while π-antibonding levels are not. In this way, the apical Al(2m)–Al(2m) bonds gain π-bonding character and show a significant increase in their overlap population, although the orbital energy changes are slight. The electron-deficient delocalized bonding between Al(1m) and Al(2m) sites is concurrently reduced.

Since the p_z orbitals in the Al(1) sites play a pivotal role in the electronic instability of the tetragonal structure via the second-order mixing term, their position in the spectrum, which is dictated by the Al(1)–Al(1) distance, is an important parameter in the prediction of whether the tetragonal structure will distort. As Table VIII shows, this distance increases from $CaAl_4$ to $BaAl_4$ by 0.145 Å, which would result in a steadily lower energy for the b_2 orbital (which has π^* character between adjacent Al(1) positions) along this sequence and, thus, a smaller e–b_2 energy gap! We contend, therefore, that both $SrAl_4$ and $BaAl_4$ may undergo a symmetry-breaking transition for reasons similar to $CaAl_4$, but at a significantly lower temperature than 170 °C.

Summary

The structural phase transformation in $CaAl_4$ at 170 °C has been identified and clarified using both high-temperature X-ray powder diffraction and room-temperature single-crystal X-ray diffraction. The results suggest that the transition from *I*4/*mmm* to *C*2/*m* is a continuous process, although we cannot rigorously prove it to have complete second-order character. Nevertheless, Landau theory provided the correct structural model for refinement of the data, and semiempirical electronic structure calculations allowed us to rationalize the transformation in terms of changes in local chemical bonding within the Al framework.

Acknowledgment. This research was supported by the U.S. Department of Energy, Office of Basic Energy Sciences, Materials Sciences Division. The Ames Laboratory is operated for the Department of Energy by Iowa State University under Contract No. W-7450-Eng-82.

Supplementary Material Available: Tables of relevant bond distances and angles in $CaAl_4$ (5 pages); a listing of F_o and F_c data for the same structure (2 pages). Ordering information is given on any current masthead page.